SPACE PHYSICS

In situ observations of large-amplitude Alfvén waves heating and accelerating the solar wind

Yeimy J. Rivera[1]*†, Samuel T. Badman[1]†, Michael L. Stevens[1], Jaye L. Verniero[2], Julia E. Stawarz[3], Chen Shi[4], Jim M. Raines[5], Kristoff W. Paulson[1], Christopher J. Owen[6], Tatiana Niembro[1], Philippe Louarn[7], Stefano A. Livi[8,5], Susan T. Lepri[5], Justin C. Kasper[9,5], Timothy S. Horbury[10], Jasper S. Halekas[11], Ryan M. Dewey[5], Rossana De Marco[12], Stuart D. Bale[13]

After leaving the Sun's corona, the solar wind continues to accelerate and cools, but more slowly than expected for a freely expanding adiabatic gas. Alfvén waves are perturbations of the interplanetary magnetic field that transport energy. We use in situ measurements from the Parker Solar Probe and Solar Orbiter spacecraft to investigate a stream of solar wind as it traverses the inner heliosphere. The observations show heating and acceleration of the plasma between the outer edge of the corona and near the orbit of Venus, along with the presence of large-amplitude Alfvén waves. We calculate that the damping and mechanical work performed by the Alfvén waves are sufficient to power the heating and acceleration of the fast solar wind in the inner heliosphere.

In situ measurements have shown that the solar wind does not cool adiabatically as it expands away from the Sun (*1*). The speed and temperature profiles of the fast solar wind (which has the highest speeds when measured far from the Sun) require mechanical forcing and direct heating of the plasma after it leaves the solar atmosphere (*2*–*4*).

The cooling rate of solar wind protons depends on the speed of each wind stream (*1*). Protons in the slowest solar wind cool roughly adiabatically as they convect away from the corona, whereas protons in faster solar wind cool more slowly (*5*). The radial electron temperature profile exhibits similar behavior, though varies less with the stream speed (*6*). Plasma that cools slower than adiabatically requires that additional heating occurs after the fast solar wind leaves the corona. The source of that heating is unknown.

Alfvén waves are transverse magnetohydrodynamic waves that travel along the magnetic field and are thought to play a role in the processes that heat the solar wind (*3*, *7*, *8*). The energy budget of the solar wind indicates that energy provided by Alfvén waves makes a greater contribution to stream acceleration at higher solar wind speeds (*4*). The acceleration of the solar wind streams with slower speeds can be explained without requiring a contribution from Alfvén waves (*9*). By contrast, Alfvén waves do contribute to the dynamics of fast solar wind (*10*, *11*).

In situ measurements by spacecraft passing close to the Sun have found high-amplitude magnetic field rotations, termed switchbacks (*12*, *13*). These switchbacks are characterized by a rapid change in the magnetic field direction, with near-constant magnetic field magnitude, accompanied by correlated velocity fluctuations. Switchbacks have been interpreted as large-amplitude Alfvén waves in the solar wind (*12*, *13*); however, their definition and implied origin are debated. Although the switchback terminology suggests a change in polarity, the magnetic field does not always physically switch back to change its magnetic polarity. Groups of many such fluctuations have been found in coherent patches (*14*). The substantial wave energy associated with these large Alfvénic fluctuations close to the Sun, and their gradual evolution with heliocentric distance, indicate that they could play a role in heating and acceleration of the solar wind (*15*, *16*).

Experimental design

A test of that hypothesis would be to measure the energy contributions in a switchback patch at points near and far from the Sun. Appropriate alignments with multiple spacecraft are rare (*17*), so statistical studies have combined measurements at similar heliocentric distances and with similar velocities (*4*, *6*, *18*). Close to the Sun, spacecraft measurements show an overall decrease in speed of all solar wind. This indicates that acceleration is taking place and the statistical approaches break down. Alternative approaches separate the solar wind into percentiles (*6*, *9*, *18*) or by combining measurements taken at several heliocentric distances (*4*), but these cannot isolate the evolution of individual plasma streams over large distances.

We investigate data from two spacecraft: Parker Solar Probe [(*19*), hereafter Parker] and Solar Orbiter (*20*). Parker orbits close to the Sun, with closest approach (perihelia) of 0.063 astronomical units (au); Solar Orbiter is located further out, with perihelia of 0.30 au. Our goal is to compare the properties and energetics of the same stream at different heliocentric distances, to determine its evolution as it moves outward from the Sun. This requires identifying conjunctions when the spacecraft intersect the same solar wind stream. We expect the Parker data taken close to the Sun to show large-amplitude Alfvén waves, whereas the Solar Orbiter data are sufficiently far out for the waves to have mostly dissipated.

Multi-spacecraft observations

A suitable conjunction occurred in February 2022, when Parker and Solar Orbiter crossed the same wind streamline at the same solar latitude within 2 days of each other. Parker crossed the stream when it was at 13.3 solar radii ($R_\odot$) from the Sun, around the outer edge of the Alfvén region, defined as the region where the solar wind is slower than the local Alfvén wave speed (*21*). The same plasma stream was subsequently crossed by Solar Orbiter at 127.7$R_\odot$, where the solar wind is much faster than the Alfvén speed.

Figure 1A shows this conjunction in the solar-corotating (Carrington) reference frame, and Fig. 1B shows the same event in longitude and latitude. We determined the source surface longitude separately for the plasmas observed at Parker and Solar Orbiter, by ballistically mapping the stream trajectories back to 2.5$R_\odot$ above the Sun according to previous methods (*22*, *23*). The ballistic mapping uses the measured wind speeds and the respective spacecraft locations to define spiral trajectories (straight lines in the rotating reference frame) that approximately trace each stream back to its point of origin in the corona (*24*–*26*).

A stream of fast wind passes by both spacecraft during this conjunction (Fig. 2 and fig. S1). The segment corresponds to source surface longitudes 120° to 125°, for which the Parker data show a patch of large-amplitude Alfvén waves, which we term a switchback patch. Parker crossed this stream on 2022 February 25 (15:00 to 16:40 Coordinated Universal Time, UTC). Solar Orbiter data show the same stream passing the spacecraft on 2022 February 27 (09:00 to 17:00 UTC). Parker crosses the same span of source longitude in

[1]Center for Astrophysics, Harvard and Smithsonian, Cambridge, MA 02138, USA. [2]NASA Goddard Space Flight Center, Greenbelt, MD 20771, USA. [3]Department of Mathematics, Physics, and Electrical Engineering, Northumbria University, Newcastle upon Tyne NE1 8ST, UK. [4]Department of Earth, Planetary, and Space Sciences, University of California, Los Angeles, CA 90095, USA. [5]Department of Climate and Space Sciences and Engineering, University of Michigan, Ann Arbor, MI 48109, USA. [6]Mullard Space Science Laboratory, University College London, Holmbury St Mary RH5 6NT, UK. [7]Institut de Recherche en Astrophysique et Planétologie, Centre National de la Recherche Scientifique, University of Toulouse, Toulouse, France. [8]Southwest Research Institute, San Antonio, TX 78228, USA. [9]BWX Technologies Inc, Washington, DC 20001, USA. [10]Department of Physics, Imperial College London, London SW7 2AZ, UK. [11]Department of Physics and Astronomy, University of Iowa, IA 52242, USA. [12]Institute for Space Astrophysics and Planetology, 00133 Rome, Italy. [13]Space Sciences Laboratory, University of California, Berkeley, CA 94720, USA.
*Corresponding author. Email: yeimy.rivera@cfa.harvard.edu
†These authors contributed equally to this work.

a much shorter time than Solar Orbiter because of its higher angular velocity, and the two spacecraft crossed the stream in opposite directions (Fig. 1B). The transit time for plasma to travel from the location of Parker to Solar Orbiter during this period was 45 hours, estimated from the modeled velocity profile (*27*), which is similar to the measured delay between Parker exiting and Solar Orbiter entering the stream (~40 hours). This implies that the plasmas encountered by Parker and Solar Orbiter were released from the Sun at roughly the same time, as well as from the same source.

The switchback patch corresponds to a local maximum in the solar wind speed and appears in both Parker and Solar Orbiter data taken over this longitude range. Further evidence of a connection between the plasma streams is provided by our identification of a positive polarity magnetic field at the same ballistically mapped longitude (120° to 125°) crossed by Parker and Solar Orbiter (fig. S1). We also find a consistent helium abundance around 1 ± 0.5% by number density (n_{He}/n_H = 0.01) in both solar wind streams (Fig. 2, E and K). We expect plasma composition to remain fixed after leaving the corona.

Over source surface longitudes 120° to 121°, there is a bifurcation in the ballistic mapping of the Solar Orbiter data, showing a solar wind stream from the same source longitude that occurs later in the time series, with a He abundance of 3% (Fig. 2K). Ballistic mapping does not account for stream interactions, so unphysically allows streams to overlap. We use the He abundance to disambiguate the fast stream from the slow stream and exclude the latter from our analysis. For both spacecraft, the fast stream of interest maps back to a small equatorial coronal hole (Fig. 2, F and L). That point of origin is consistent with the heavy-ion abundances measured by Solar Orbiter (fig. S4), which are typical of coronal holes (*27*).

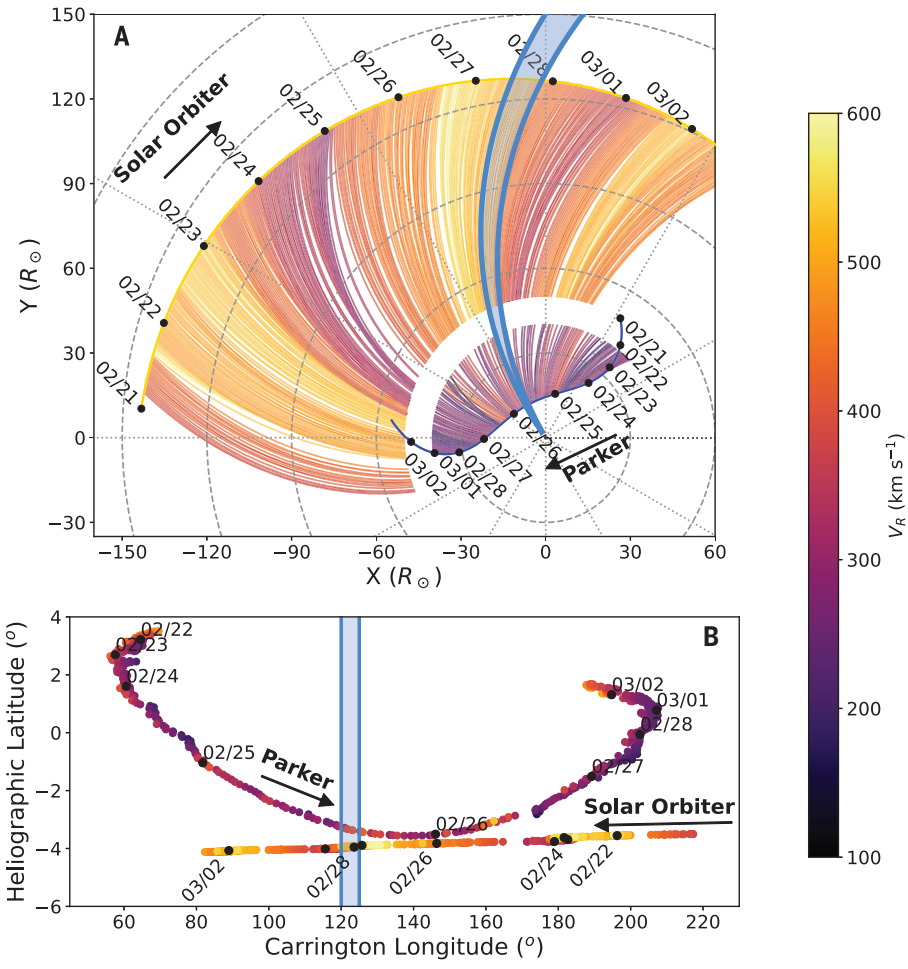

Fig. 1. Spacecraft trajectories and ballistic mapping in the corotating reference frame. (**A**) Solar Orbiter and Parker trajectories projected onto the solar equatorial plane (Cartesian coordinates X and Y with the origin at the Sun). Spiral streamlines are colored with the measured solar wind speed; they show the mapping of the spacecraft measurements to the Sun, with a gap separating the segments generated from Solar Orbiter (outer segment) and Parker data (inner segment). Dotted and dashed lines show uniform spacing in longitude and radius, respectively. Black arrows indicate the direction of spacecraft motion. The blue shaded region indicates the fast solar wind stream that we study. Black circles indicate spacecraft positions on the labeled dates (month/day); the connecting yellow and dark blue lines are the projected spacecraft trajectories. (**B**) The mapped heliographic coordinates (longitude and latitude) of Parker and Solar Orbiter at 2.5$R_\odot$, with Parker's latitude shifted up 0.3° for display. Colors and plotting symbols are the same as in (A).

Evolution of the plasma stream

The plasma stream has different speeds at the two spacecraft, with the Parker data averaging 386 ± 26 km s^{-1} and the Solar Orbiter data 512 ± 15 km s^{-1} (table S1). We consider the latter stream to be fast solar wind, even though the speed at Parker would be classified with slow solar wind if it were observed at Earth. The stream has undergone acceleration during its passage from 13.3$R_\odot$ to 127.7$R_\odot$ from the Sun.

We compared the mass flux and magnetic flux at the two spacecraft to verify whether these quantities are conserved (*27*), as we expect for an expanding flux tube. We find that both quantities are conserved and that the stream compresses slightly more than the $1/r^2$ variation that we expect for a flux tube (fig. S2). We calculate a 10 ± 9% compression factor at Solar Orbiter (eqs. S1 and S2). For the energy flux budget of the stream, we calculate that energy is conserved (within the measurement uncertainties), and that the dominant source of uncertainty is the variance of the stream over the source surface longitude. The energy flux is 45.7 ± 6.6 W m^{-2} at Parker and 48.0 ± 3.6% W m^{-2} at Solar Orbiter (table S2).

We express the conservation of energy along the flux tube as

$$W_{\text{SolarOrbiter}} - W_{\text{Parker}} = \Delta W = \Delta\left[u_{\text{cm}}\Omega\frac{r^2}{R_\odot^2}(U_K + U_H + U_G + U_w)\right] \quad (1)$$

$$= \Delta W_K + \Delta W_H + \Delta W_G + \Delta W_w \quad (2)$$

$$= 0 \quad (3)$$

where ΔW is the difference between energy fluxes at Parker and Solar Orbiter and the subscripts indicate kinetic (K), enthalpy (H), gravitation (G), and Alfvénic wave (w) energies. u_{cm} is the plasma center of mass velocity, computed as $u_{\text{cm}} = \sum_j m_j n_j v_j \sum_j m_j n_j$, where j indexes each species: electrons, protons, and alpha particles. Ω is the stream angular size in steradians at each spacecraft. Each energy density term (U) corresponds to a scaled energy flux term (W) once normalized by $u_{\text{cm}} r^2/R_\odot^2$, where r is the heliocentric

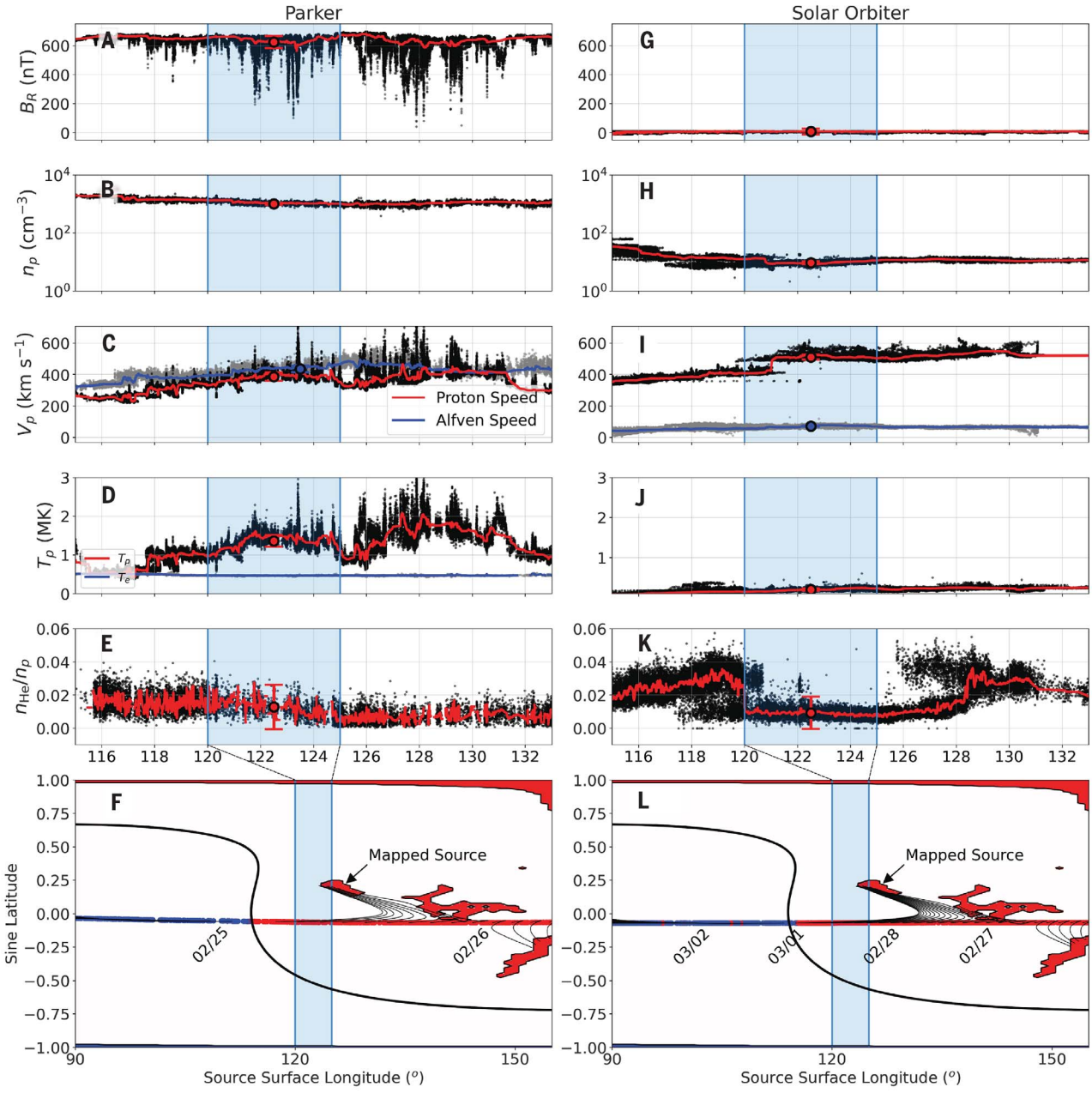

Fig. 2. Solar wind properties measured by Parker and Solar Orbiter across source surface longitude. Each row shows equivalent data from Parker (A to F) and Solar Orbiter (G to L), and the blue shaded region indicates the fast solar wind stream that we study. (**A** and **G**) Radial magnetic field component; (**B** and **H**) proton density; (**C** and **I**) proton bulk speed (red) and Alfvén velocity (blue); (**D** and **J**) isotropic proton temperature (red) and electron temperature (blue, Parker only); (**E** and **K**) helium to proton number density ratio. The black points show the measured values, whereas red solid curves are smoothed with a 50-point median filter. For panels where a second measurement is shown [(C), (D), (I), and (J)], the data and median filter are differentiated with gray points and a blue solid curve, respectively. Large circles with error bars (1σ uncertainty) are averaged values (table S1). (**F** and **L**) Coronal hole source mapping. Colored points indicate the mapped positions where B_R is positive (red) or negative (blue); labels indicate dates (month/day). Black lines are field lines from a potential field source surface (PFSS) model, linking the trajectory at the source surface to their solar sources at 1 $R_\odot$, indicated by solid red and blue regions with black contours. The solid black curve shows the polarity inversion line. Both spacecraft map to the same location (black arrows), which is consistent with the measured in situ compositional context (*27*).

distance (*28*). Each U and W term includes contributions from electrons, protons, and alpha particles.

This formulation does not explicitly include the ambipolar electric potential induced by hot electrons escaping the Sun's corona; that energy is included in the electron thermal pressure or the enthalpy (U_H) (*4*, *9*). Equations 1 to 3 indicate that the total energy transported through a cross-sectional area Ωr^2 at center-of-mass velocity u_{cm} is equal at both spacecraft. We compute the contributions of each term from the Parker and Solar Orbiter measurements (*27*). We assume $\Omega = 1$ at Parker and compute an equivalent expansion factor (f)

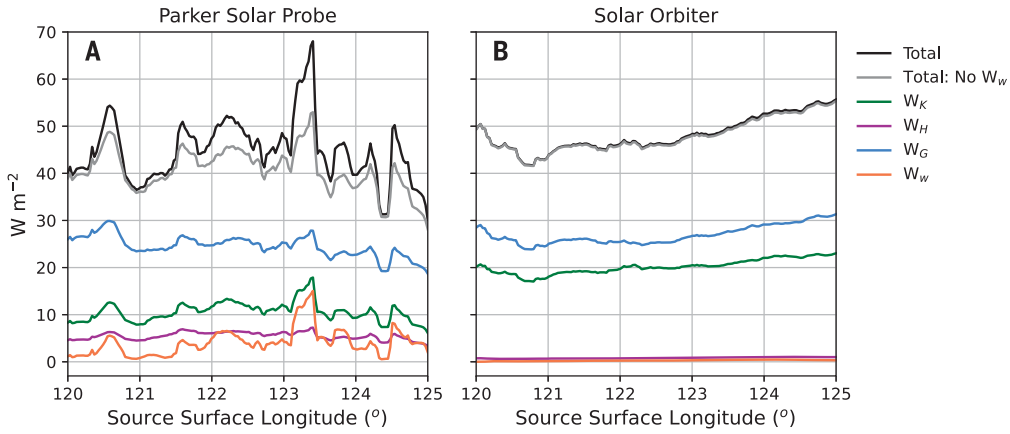

Fig. 3. Energy fluxes across the fast wind stream. The individual energy flux terms are shown for (**A**) Parker and (**B**) Solar Orbiter multiplied by the expansion factor f (*27*). Colored lines show the energy flux terms in Eq. 2. The black line is their total, and the gray line is the total without including energy from the Alfvén waves. We conclude that the switchback wave energy at Parker is required to maintain energy conservation.

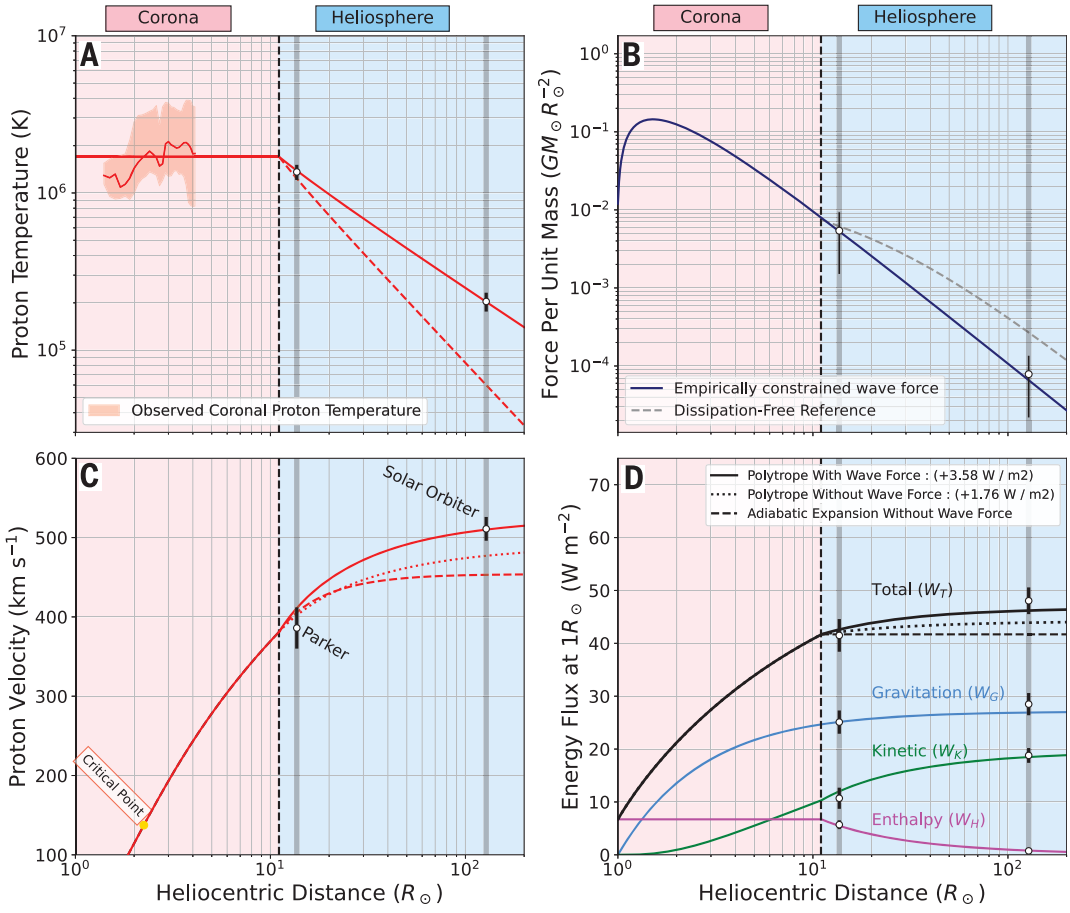

Fig. 4. Comparison of measured properties with a solar wind model as a function of heliocentric distance. White data points (error bars show 1σ uncertainties) are our measurements from Parker and Solar Orbiter (tables S1 and S2). The curves are model results (*27*). Each model is split (at the vertical dashed line) into coronal and heliospheric portions (pink and blue shading, respectively). (**A**) Proton temperature for polytropic (solid red line) and adiabatic (dashed red line) expansion. Red shading and a second red line show remote observations of fast wind low in the corona (*31*). (**B**) Wave pressure gradient force, using a data-constrained analytical model (solid blue line) and a dissipation-free model (dashed gray line). (**C**) Proton velocity for adiabatic expansion only (dashed red line), polytropic expansion only (red dotted line), and polytropic expansion and wave pressure (solid red line). The yellow circle indicates the critical point. (**D**) The energy flux terms for enthalpy (magenta line), kinetic (green line), and gravitation (blue line). Their total (black lines) is shown for each of the three expansion models, with line styles as in (C).

at Solar Orbiter through consideration of mass flux conservation (*27*).

The resulting energy flux terms are shown as a function of source surface longitude for Parker (Fig. 3A) and Solar Orbiter (Fig. 3B). We find that energy conservation is satisfied to within the uncertainty of the total energy flux, but only when wave energy is included. Uncertainties are computed as the standard deviation of the energy flux terms across the 5° source surface longitude range. The instrumental uncertainties are smaller than the intrinsic variability of the measurements. The overall wave energy term is of similar magnitude to the total energy flux variability but contributes a substantial part of the energy budget at Parker, and its inclusion is required to maintain energy conservation between the locations of the two spacecraft (table S2).

Acceleration and heating of the stream

If we assume that the stream did not change in time over this period and that the plasma has a polytropic equation of state, then the expansion profile for the stream of solar wind is fully determined by hydrodynamics (*29*, *30*).

Following previous methods (*5*, *6*, *29*), we extrapolate from the Parker and Solar Orbiter observations using a polytrope function, $P\rho^{-\gamma} = C$, where P is the plasma thermal pressure, ρ is the mass density, γ is the polytropic index, and C is an unknown constant. Figure 4 shows the resulting proton temperature, wave pressure force, and proton speed profiles, along with the energy flux evolution of the stream. Figure 4, C and D, compare three choices of polytrope: (i) free adiabatic expansion, $\gamma = 5/3$; (ii) a polytrope in which the temperature was derived from a model fitted to the observations, $\gamma = 1.41 \pm 0.020$; and (iii) the same fitted polytrope with the addition of the empirically constrained wave pressure force profile (*27*). In the latter case, the mechanical work performed by the Alfvén waves was determined from an analytical force profile (*5*) (Fig. 4B), which is consistent with the measured gradient in Alfvénic wave pressure (*27*).

Figure 4 also shows extrapolations of these polytrope models into the corona, where we assume the temperature profile (Fig. 4A) is approximately constant, as described in previous work (*29*). The temperature profiles consist of a constant proton temperature $T_{iso} = 1.7 \times 10^6$ K (Fig. 4A), which is combined with the wave pressure force profile (Fig. 4B) within a radius of $R_{iso} = 11R_\odot$, measured from the center of the Sun. These parameters were chosen on the basis of ultraviolet remote observations of the fast solar wind temperature in the corona (*31*). They are consistent with other remote observations that showed that the sonic critical point, where the solar wind speed exceeds the local sound speed, is located at 1.9 $R_\odot$ (*32*), near our modeled value of $2.2R_\odot$ (Fig. 4C). We extrapolate the coronal wave pressure forcing (Fig. 4B), finding that it contributes about 20 W m^{-2} to the energy budget, compared with the 120 W m^{-2} present at the base of the corona (*33*). This extrapolation to the corona indicates that our results are consistent with the expected physical parameters of the corona. Under our assumed isothermal conditions in the corona, the plasma still receives energy from the Alfvén waves, but it exactly balances the cooling due to expansion.

Figure 4, C and D, show the effect of the Alfvén wave energy flux on the system. All three polytrope models start from the same initial conditions at R_{iso}, but only the polytrope that includes both Alfvén wave pressure forcing and heating matches the measured acceleration between Parker and Solar Orbiter (Fig. 4C). We estimate the mechanical work done from the measured decline in wave pressure (1.88 ± 0.31 W m^{-2}) and from the shallower-than-adiabatic thermal pressure gradient of the polytropic heating profile (1.76 ± 0.25 W m^{-2}). The portion of the wave energy flux resulting in acceleration (1.88 ± 0.31 W m^{-2}) is substantially less than the mean of the total wave energy flux lost (3.9 ± 2.7 W m^{-2}). This implies that the large-amplitude Alfvén waves are damped. If there was no damping, then all the wave energy flux would be converted to mechanical work, so the wave force profile would be shallower and follow the dissipation-free curve (Fig. 4B) (*3*, *7*, *34*). The unused wave energy flux is similar to the energy input required to sustain the temperature profile with our fitted polytropic index. We speculate that the waves are converted to heat through a combination of reflection-driven turbulence (*8*, *35*) and turbulent dissipation (*36*–*38*).

These observations show that substantial heating and acceleration of the plasma, above that expected for free adiabatic expansion (3.62 ± 0.40 W m^{-2}), occurred in this region. The large-amplitude Alfvén waves organized in coherent patches dissipate 3.9 ± 2.9 W m^{-2} into the stream. These Alfvénic structures can therefore provide the necessary additional heating and acceleration as the solar wind moves through the corona and inner heliosphere.

REFERENCES AND NOTES

1. P. Hellinger, L. Matteini, Š. Štverák, P. M. Trávníček, E. Marsch, *J. Geophys. Res. Space Phys.* **116**, A09105 (2011).
2. E. N. Parker, *Space Sci. Rev.* **4**, 666 (1965).
3. G. Alazraki, P. Couturier, *Astron. Astrophys.* **13**, 380 (1971).
4. J. S. Halekas *et al.*, *Astrophys. J.* **952**, 26 (2023).
5. C. Shi *et al.*, *Phys. Plasmas* **29**, 122901 (2022).
6. J.-B. Dakeyo, M. Maksimovic, P. Démoulin, J. Halekas, M. L. Stevens, *Astrophys. J.* **940**, 130 (2022).
7. J. W. Belcher, *Astrophys. J.* **168**, 509 (1971).
8. B. D. G. Chandran, J. V. Hollweg, *Astrophys. J.* **707**, 1659–1667 (2009).
9. J. S. Halekas *et al.*, *Astrophys. J.* **936**, 53 (2022).
10. V. Réville *et al.*, *Astrophys. J. Suppl. Ser.* **246** (Supp.), 24 (2020).
11. M. Shoda, B. D. G. Chandran, S. R. Cranmer, *Astrophys. J.* **915**, 52 (2021).
12. S. D. Bale *et al.*, *Nature* **576**, 237–242 (2019).
13. J. C. Kasper *et al.*, *Nature* **576**, 228–231 (2019).
14. S. D. Bale *et al.*, *Astrophys. J.* **923**, 174 (2021).
15. A. Tenerani *et al.*, *Astrophys. J. Lett.* **919**, L31 (2021).
16. V. K. Jagarlamudi *et al.*, *Astrophys. J. Lett.* **950**, L7 (2023).
17. S. J. Schwartz, E. Marsch, *J. Geophys. Res.* **88**, 9919–9932 (1983).
18. M. Maksimovic *et al.*, *Astrophys. J. Suppl. Ser.* **246** (supp.), 62 (2020).
19. N. J. Fox *et al.*, *Space Sci. Rev.* **204**, 7–48 (2016).
20. D. Müller *et al.*, *Astron. Astrophys.* **642**, A1 (2020).
21. J. C. Kasper *et al.*, *Phys. Rev. Lett.* **127**, 255101 (2021).
22. D. Stansby, T. S. Horbury, S. Wallace, C. N. Arge, *Res. Not. Am. Astron. Soc.* **3**, 57 (2019).
23. S. T. Badman *et al.*, *Astrophys. J. Suppl. Ser.* **246**, 23 (2020).
24. J. T. Nolte, E. C. Roelof, *Sol. Phys.* **33**, 241–257 (1973).
25. A. R. Macneil, M. J. Owens, A. J. Finley, S. P. Matt, *Mon. Not. R. Astron. Soc.* **509**, 2390 (2022).
26. J. B. Dakeyo *et al.*, *Astron. Astrophys.* **686**, A12 (2024).
27. Materials and methods are available as supplementary materials.
28. M. Liu *et al.*, *Astron. Astrophys.* **650**, A14 (2021).
29. E. N. Parker, *Astrophys. J.* **128**, 664 (1958).
30. E. N. Parker, *Astrophys. J.* **132**, 821 (1960).
31. S. R. Cranmer, *Astrophys. J.* **900**, 105 (2020).
32. D. Telloni, S. Giordano, E. Antonucci, *Astrophys. J. Lett.* **881**, L36 (2019).
33. B. De Pontieu *et al.*, *Science* **318**, 1574–1577 (2007).
34. S. A. Jacques, *Astrophys. J.* **215**, 942 (1977).
35. A. A. van Ballegooijen, M. Asgari-Targhi, *Astrophys. J.* **821**, 106 (2016).
36. L. Sorriso-Valvo *et al.*, *Phys. Rev. Lett.* **99**, 115001 (2007).
37. B. T. MacBride, C. W. Smith, M. A. Forman, *Astrophys. J.* **679**, 1644–1660 (2008).
38. J. E. Stawarz, C. W. Smith, B. J. Vasquez, M. A. Forman, B. T. MacBride, *Astrophys. J.* **697**, 1119–1127 (2009).
39. S. T. Badman *et al.*, ParkerSolarWind, Zenodo (2023); https://doi.org/10.5281/zenodo.10257870.

ACKNOWLEDGMENTS

Parker Solar Probe was designed, built, and is now operated by the Johns Hopkins Applied Physics Laboratory as part of NASA's Living with a Star (LWS) program (contract NNN06AA01C). The SWEAP Investigation is a multi-institution project led by the Smithsonian Astrophysical Observatory in Cambridge, Massachusetts. Other members of the SWEAP team come from the University of Michigan, University of California, Berkeley Space Sciences Laboratory, The NASA Marshall Space Flight Center, The University of Alabama Huntsville, the Massachusetts Institute of Technology, Los Alamos National Laboratory, Draper Laboratory, JHU's Applied Physics Laboratory, and NASA Goddard Space Flight Center. The FIELDS instrument suite was designed and built and is operated by a consortium of institutions including the University of California, Berkeley; University of Minnesota; University of Colorado, Boulder; NASA/GSFC, CNRS/LPC2E, University of New Hampshire, University of Maryland, UCLA, IFRU, Observatoire de Meudon, Imperial College, London, and Queen Mary University London. Solar Orbiter is a mission of international collaboration between ESA and NASA, operated by ESA. The Solar Orbiter Solar Wind Analyser (SWA) data are derived from scientific sensors that have been designed and created by, and are operated under funding provided in numerous contracts from, the UK Space Agency (UKSA), the UK Science and Technology Facilities Council (STFC), the Agenzia Spaziale Italiana (ASI), the Centre National d'Etudes Spatiales (CNES, France), the Centre National de la Recherche Scientifique (CNRS, France), the Czech contribution to the ESA PRODEX program and NASA. The Solar Orbiter magnetometer was funded by the UK Space Agency (grant ST/T001062/1). **Funding:** Y.J.R. acknowledges support from the Future Faculty Leaders postdoctoral fellowship at Harvard University and NASA grant NNN06AA01C. S.T.B., M.L.S., K.W.P., T.N., S.D.B., and J.S.H. acknowledge support from NASA grant NNN06AA01C. R.M.D. acknowledges support from NASA grant 80NSSC22K0204. J.L.V. acknowledges support from NASA PSP-GI grant 80NSSC23K0208 and NASA LWS grant 80NSSC22K1014. J.E.S. was supported by the Royal Society University Research Fellowship URF\R1\201286. S.A.L. was funded by NASA contract NNG10EK25C. Funding for S.T.L. and J.M.R. was provided through SwRI subcontract A99201MO to the University of Michigan. T.S.H. was supported by STFC grant ST/W001071/1. C.J.O., P.L., and R.D.M. were supported by STFC grants ST/T001356/1 and ST/S000240/1. J.S.H. was supported by NASA grant 80NSSC22K1014. **Author contributions:** Y.J.R. and S.T.B. were jointly responsible for the conceptualization, formal analysis, and writing the manuscript. M.L.S, K.W.P., T.N., C.S., and T.S.H. helped conceive and design the study. J.E.S., R.D.M., and J.S.H. contributed interpretation of the spacecraft data. J.L.V., R.M.D., S.A.L., P.L., C.J.O., J.C.K., T.S.H., S.D.B., J.M.R., and S.T.L. performed data acquisition. All authors commented on the manuscript. **Competing interests:** The authors declare no conflicts of interest. **Data and materials availability:** For Parker Solar Probe the SWEAP data are available at http://sweap.cfa.harvard.edu/pub/data/sci/sweap/spi/L2/spi_sf00/2022/02/ and the FIELDS data at https://research.ssl.berkeley.edu/data/psp/data/sci/fields/l2/mag_RTN_4_Sa_per_Cyc/2022/02/; in both cases, we used the .cdf files with "20220225" in the file names. The Solar Orbiter data are available at https://soar.esac.esa.int/soar/#search; we used the .cdf files from 2022 February 27 for instruments MAG and SWA, with processing level L2. Our modeling code is available at https://github.com/STBadman/ParkerSolarWind and archived at Zenodo (*39*). Our measured properties of the stream are listed in table S1, and the results of our energy budget calculations are in table S2.

SUPPLEMENTARY MATERIALS

science.org/doi/10.1126/science.adk6953
Materials and Methods
Supplementary Text
Figs. S1 to S4
Tables S1 and S2
References (*40*–*58*)

Submitted 5 September 2023; accepted 3 July 2024
10.1126/science.adk6953